

Molecular Mechanism of HF Acid Ionization in Water: An Electronic Structure–Monte Carlo Study

Koji Ando*,†

Institute of Materials Science, University of Tsukuba, Tsukuba, Ibaraki 305-8573, Japan

James T. Hynes*,‡

Department of Chemistry and Biochemistry, University of Colorado, Boulder, Colorado 80309-0215

Received: July 17, 1999; In Final Form: September 24, 1999

The results of a theoretical study of the acid ionization to form first a contact ion pair and then a solvent-separated ion pair are presented for HF in water. The ionization reaction to produce the contact ion pair is found to involve adiabatic quantum proton transfer (PT) and has an activation barrier in a collective solvent reaction coordinate of 2.9 kcal/mol, with a positive reaction free energy estimated as 2.2 kcal/mol. This result identifies the weakness of HF acid in aqueous solution as arising from this intrinsic acid ionization step, rather than from the thermodynamic difficulty of separating the ions so produced. The calculated charge distributions for the first step are in support of the unconventional Mulliken picture for PT. The second step to produce a solvent-separated ion pair is found to be sequential in connection with the first step, rather than concerted, and is also a quantum adiabatic PT. This reaction step proceeds via a solvent reaction coordinate and is slightly activated. The two step sequence in reverse order is discussed in connection with the Eigen picture of acid–base recombination in aqueous solution.

1. Introduction

The ionization (and recombination) reaction of an acid in water, $\text{HA}(\text{aq}) \rightleftharpoons \text{A}^-(\text{aq}) + \text{H}_3\text{O}^+(\text{aq})$, is particularly important in chemistry and biochemistry, both per se and in connection with acid–base catalysis.^{1–5} However, the microscopic mechanism of this elementary reaction in solution has received fairly limited attention from a theoretical perspective.^{6–22} In previous publications, we have described a theoretical and computational approach to elucidate the molecular mechanism of the ionization of hydrochloric acid ($\text{A} = \text{Cl}$) in water,^{10–13} an approach later extended to HCl acid ionization at an ice surface.²³ In this work, we present the corresponding analysis for hydrofluoric acid ($\text{A} = \text{F}$).

While HF and HCl are obviously in the same family of acids, one major experimental difference between these two acids is that HF is a comparatively weak acid with $\text{p}K_{\text{a}} \approx +3$ in water; i.e., the ionization has a positive free energy of reaction, while HCl is a strong acid ($\text{p}K_{\text{a}} \approx -7$) with a negative reaction free energy of ca. -10 kcal/mol. The latter acid was estimated by us^{10,11} to have little or no barrier for reaction to produce a contact ion pair between Cl^- and H_3O^+ , such that this step would be very rapid and quite difficult to study experimentally. The $\text{p}K_{\text{a}}$ comparison however suggests that the PT to water in the HF ionization would be much slower than that for HCl, with an activation free energy at least equal to the reaction free energy for the formation of a contact ion pair; thus the microscopic dynamics for the HF reaction could be more directly accessible via modern experimental methods.

A theoretical study of the HF acid ionization in water is of interest for a further reason. On the basis of some spectroscopic

studies of this reaction in fairly concentrated aqueous HF solutions, it has been proposed¹⁷ that the weakness of the acidity of HF is not due to the source(s) to which it is customarily attributed, e.g. to the strength of the HF bond.²⁴ Instead, it is suggested that the formation of a contact $\text{F}^- \cdots \text{H}_3\text{O}^+$ ion pair is strongly thermodynamically favored in water and that the weakness of HF as an acid instead arises from the thermodynamically disfavored separation of this ion pair into the separated ions.¹⁷ This fundamental issue connected to what is perhaps the simplest class of acids appears to have been largely ignored, but in our view deserves attention.

The HF acid ionization reaction can also be used to study two further issues of interest. The first is the question of the applicability of the Mulliken picture^{25,26} of the electronic character of proton transfer reactions, an unconventional charge transfer view in which charge flows from the proton-accepting base to the proton-donating acid, coupled with transfer of a protonic species having attributes of an H atom. The second is the possibility of mode selective chemistry in solution attained via vibrational excitation of the HF acid.

The basic perspective of our approach, which has been detailed and supported in ref 11 (and in refs 6–9 for related nonaqueous PTs), is summarized as follows. First, due to strong electrostatic coupling of the polar solvent to the ionization, the solvent fluctuation and reorganization are expected to be key to the reaction mechanism. In a fashion analogous, but not identical,^{11,27} for electron transfer reactions in polar solvents,²⁸ in which the free energy surface crossing induced by the fluctuation of the polar environment is essential, we invoke the following scheme for proton transfers: the proton potential and its asymmetry are modulated by the fluctuating polar environment, and the PT occurs at the crossing point of the solvent configuration which gives a, symmetric proton potential (see,

† E-mail: ando@ims.tsukuba.ac.jp, Fax: 81-298-55-7440.

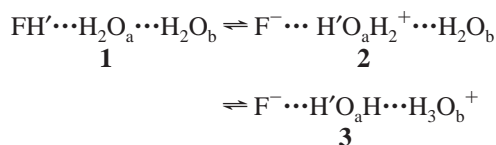
‡ E-mail: hynes@spot.colorado.edu, Fax: 303-492-5894.

e.g. Figure 1 in ref 11). The asymmetry modulation of the proton potential could be comprehended in terms of a valence-bond (VB) picture,⁸ closely related to the Mulliken view of PT:²⁵ For example, for the first PT step of HF ionization, the relative stability of the neutral ($\text{FH}\cdots\text{OH}_2$) and the ionic ($\text{F}^-\cdots\text{HOH}_2^+$) VB states varies depending on the degree of solvent (nuclear) polarization, which causes alteration of the proton potential curve. (The very strong electronic coupling between these electronic VB states—related to the fact that bonds are broken and made—is one important difference, among others, between proton transfer and electron transfer.¹³) Since solvent activation is generally required to attain the crossing point, there can be a free energy barrier in the reaction coordinate whose major component consists of the solvent motion.

Second, we take account of the essential quantized nature of the proton motion.^{10,11} Depending on the strength of the hydrogen-bonding interaction, the height of the proton potential barrier and the position of the quantized proton vibrational energy levels (at the crossing point mentioned above) may vary. For weak hydrogen-bonding complexes in which the proton barrier is higher than the (split) ground proton vibrational levels, the PT will be a quantum tunneling process. In the case of strong hydrogen bonding, in which the equilibrium distance separating the heavy partners between which the PTs is smaller, the proton barrier top is located below the ground proton vibrational level, and the PT is no longer tunneling, although it is still completely quantum. We call this an adiabatic PT: the proton wavepacket motion adiabatically follows the modulation of the proton potential from the reactant solvent configuration through the crossing point to the product state. The distance between the heavy atoms between which the PTs can be important in allowing this adiabatic pathway.

Third, as in ref 11, we consider the Grotthuss mechanism of PTs in aqueous media, that is, in our case, the question of whether the double PT in Scheme 1 is stepwise ($\mathbf{1} \rightarrow \mathbf{2} \rightarrow \mathbf{3}$) or concerted ($\mathbf{1} \rightarrow \mathbf{3}$). We will conclude that the double PT is stepwise, as for HCl.^{10,11} As was the case for HCl, the second step shares some characteristics with the problem of proton transport in water, a topic receiving much current attention.²⁹

Scheme 1



Finally, as implied above, additional issues to be addressed, which did not arise in the previous work on the strong acid HCl, are whether the weakness of HF as an acid is reflected in the first ionization step to produce a contact ion pair or has a different source, and the character of the ion recombination process to produce the weak molecular acid HF. Our results support the first interpretation. (Indeed, the endothermic character of this step, as well as the need to address the inherent quantum nuclear character of the proton, makes the HF ionization problem difficult to treat via the relatively short time scale of the simulation by ab initio molecular dynamics methods.¹⁸) Further, the possibility of infrared induced HF ionization is briefly sketched, based on the free energy curves for the vibrationally excited proton state along the solvent coordinate.

The outline of the remainder of this paper is as follows. After summarizing the computational methods in the next section, we discuss in section 3 the results of the solvent free energies

and the proton potentials for the first and second PT steps, including discussion of the applicability of the Mulliken picture of PT. The issues of the stepwise versus concerted pathway of the double PT are addressed in section 4. The origin of the weakness of HF acid and the possibility of IR-induced PT are also discussed. Remarks on the character of the ion pair recombination process based on the present results are given in section 5. A final section concludes. A preliminary discussion focused on some aspects of the first proton transfer step has appeared;¹² some perspective may be found there on the HF ionization reaction in the context of $\text{S}_{\text{N}}1$ and $\text{S}_{\text{N}}2$ reactions, for which Kent Wilson and the senior author have collaborated in simulation studies in the past.³⁰

2. Computational Procedures

Since the computational procedures are almost identical to those developed previously for HCl ionization in water, we give here only a compressed summary and refer to ref 11 for further details. The structural and energetic parameters used in the simulations are however presented here.

Ab initio molecular orbital (MO) methods³¹ are used in several different ways in different stages of the overall procedure: (i) to optimize the nuclear geometries of small clusters, (ii) to determine the model potential parameters for Monte Carlo simulations, and (iii) ultimately to compute the potential energy surfaces as a function of proton coordinates.

We first optimize the geometry of the reaction system **1** surrounded by eight water molecules (see Figure 2 of ref 11). The eight external waters constitute the nearest-neighbor solvation around **1**—each of the three (HF , H_2O_a , and H_2O_b) is coordinated by four molecules. In practice, the geometries of smaller four-hydrated clusters are optimized one by one rather than carrying out the full calculation of the whole system (see ref 11 for details). The analytic gradient method for the restricted Hartree–Fock (RHF) wave function³² is employed with the 3-21G* basis set,³³ in which the exponents of the d-polarization functions on O and F atoms are both 0.8. The optimized heavy atom distances $\text{F}\cdots\text{O}_a$ and $\text{O}_a\cdots\text{O}_b$, and the $\text{F}-\text{H}$ (r_1) and O_a-H (r_2) bond lengths are 2.57, 2.83, 0.97, and 0.98 Å, respectively.

We have also examined the cluster structure change associated with successive hydration of HF, i.e., $\text{HF}(\text{H}_2\text{O})_n$ with $n = 0 \rightarrow 4$. A reduction of the $\text{F}\cdots\text{O}_a$ distance (2.643, 2.589, 2.549, and 2.468 Å for $n = 1, 2, 3$, and 4) and an extension of the $\text{F}-\text{H}$ bond length (0.923, 0.934, 0.941, 0.953, and 0.974 Å for $n = 0, 1, 2, 3$, and 4) is observed. These indicate an enhancement of the polarity of HF, which would be attributed to an increase of the ionic component compared to a neutral one in a simple VB language.⁸

Monte Carlo (MC) simulations are carried out to determine the free energies in the solvent coordinate. Each cubic cell, under periodic boundary conditions, contains the solute **1**, **2**, or **3** and 248 solvent water molecules. The temperature is fixed at 298 K in generating the canonical (constant NVT) ensemble by Metropolis sampling.³⁴ The box length is 19.6 Å, so that the mass density of the system is 0.997 g/cm³. The free energy curves are computed from several (4–8) sets of 1×10^6 configurations generated after sufficient equilibration runs. The intermolecular interactions are spherically truncated at a cutoff distance of half the box length, referencing to the center-of-mass distance of each molecule.

Under certain solvent configurations identified in sections 3 and 4, and alluded to at the conclusion of this section, we calculate the potentials for the proton transfers as a function of the proton coordinate by the single and double excitations

TABLE 1: Point Charge Parameters^a

	1	2	3
F	-0.610 (-0.528)	-0.895 (-0.839)	-0.924 (-0.886)
H ₁	0.523 (0.425)	0.456 (0.434)	0.464 (0.445)
O _a	-0.982 (-0.791)	-0.702 (-0.612)	-0.974 (-0.846)
H ₂	0.519 (0.425)	0.554 (0.481)	0.451 (0.414)
H ₃	0.519 (0.425)	0.554 (0.481)	0.524 (0.422)
O _b	-0.965 (-0.800)	-0.969 (-0.805)	-0.627 (-0.547)
H ₄	0.498 (0.422)	0.501 (0.430)	0.543 (0.499)
H ₅	0.498 (0.422)	0.501 (0.430)	0.543 (0.499)

^a Values in parentheses are for the isolated trimers **1–3**.

configuration interaction (CI(SD)) method³⁵ with the 6-31G**-(F+) basis set. The exponents of the d-polarization functions on O and F atoms are the same as in the 3-21G* set, and that of the p-polarization function on H atom is 1.0. A set of p-type diffuse functions³⁶ with the exponent of 0.074 is also placed on the F atom to better describe the diffuse anion F⁻. In the CI(SD) calculations, the lowest 23 orbitals, which constitute the “minimal space” plus three Rydberg-type orbitals, are chosen for the CI space. The lowest three orbitals representing the 1s cores of F and O atoms are kept doubly occupied (frozen). The number of configuration state functions is then 4753. We included the Davidson’s correction³⁷ for the CI(SD) energy.

We determine model potential parameters for the simulations in the form of pairwise Coulomb plus 12-6 Lennard-Jones (LJ) potentials between atomic centers.³⁸ We employ the TIP3P parameters³⁹ for the external solvent waters. The charge parameters for the solute states **1–3** are determined so as to reproduce the electrostatic potentials at ~500 points around the solute computed from the RHF/6-31G**-(F+) wave function. To account for the solvent-induced polarization of the solute, RHF/6-31G**-(F+) calculations are repeated under the influence of the classical point charges of the eight externals reorganized to each charge distribution of the (isolated) systems **1–3**. The resulting charge parameters are listed in Table 1. For comparison, the charges for the isolated **1–3** are also included and show the solvent-induced polarization of the system. It is also worth pointing out that the net charge on F atom in states **2** and **3** is -0.895 and -0.924 rather than a unit negative charge, indicating a certain charge delocalization throughout the system.

The LJ energy and length parameters ϵ and σ are determined so as to reproduce the interaction energies and the average heavy atoms (F...O and O...O) distances for clusters HF(H₂O)₄, F⁻(H₂O)₄, and H₃O⁺(H₂O)₃. The reference energies and geometries are taken from MP2/6-31G**-(F+) energy calculations and RHF/3-21G* geometry optimizations. (MP2 denotes the second-order Møller–Plesset perturbation method.⁴⁰) The determined parameters and the reference quantities are summarized in Table 2.

To further check the model potential functions, radial distribution functions (rdfs) are computed from MC simulations of F⁻ ion isolated in water. As shown in ref 11, our parametrization procedure gives the rdfs around Cl⁻ in water in reasonable agreement with experimental X-ray and neutron diffraction data and with previous simulation results. However, due to lack of experimental data for F⁻ in water, we can presently argue only by comparison with the previous simulation works by others.⁴¹ The first peaks in the ion–oxygen and ion–hydrogen rdfs were found at 2.7 and 1.8 Å, while the previous simulation results are dispersed within the ranges 2.2–2.67 and 1.2–1.73 Å, respectively. The coordination numbers of F⁻ (defined by integration to the minimum after the first peak) are 6.8 and 6.6 from the ion–oxygen and ion–hydrogen rdfs, compared to 4.09–6.3 from the previous works.

TABLE 2: Lennard-Jones Parameters σ and ϵ in the Potential Form $4\epsilon_{ab}\{(\sigma_{ab}/r_{ab})^{12} - (\sigma_{ab}/r_{ab})^6\}$

	HF	F ⁻	H ₃ O ⁺
n	4	4	3
\bar{R}_{OX} (ref) ^a	2.73	2.58	2.58
\bar{R}_{OX} (model)	2.70	2.61	2.58
V_{int} (ref) ^b	-34.2	-77.1	-90.2
V_{int} (model)	-33.3	-78.4	-90.3
σ_{OX} (Å)	2.85	3.77	2.63
ϵ_{OX} (kcal/mol)	0.295	0.0191	2.44

^a Average aqueous oxygen–X atoms distance (in Å, X = F or O) in the hydration clusters with n waters computed from the RHF/3-21G* geometry optimizations. ^b MP2 hydration energies in kcal/mol calculated with the 6-31G**-(F+) basis set for HF, F⁻, or H₃O⁺ and the 6-31G* set for water.

The solvent coordinate is defined by the energy difference of the states **1–3**

$$\Delta E_{ij} \equiv V_i(\mathbf{S}; \mathbf{R}_i) - V_j(\mathbf{S}; \mathbf{R}_j)$$

where $V_i(\mathbf{S}; \mathbf{R}_i)$ denotes the total potential energy (including the solute internal and solute–solvent and solvent–solvent interaction energies) at a fixed solute coordinate \mathbf{R}_i ,⁴² as a function of the solvent configuration \mathbf{S} . This ΔE coordinate gauges the relative energetics of two solute states at a given solvent configuration, which in other words reflects degree of the solvent polarization when there exists large polarity difference between the two states. The subscripts i and j denote the diabatic states corresponding to **1–3**. Therefore, $(i, j) = (1, 2)$ and $(2, 3)$ represent the first and the second PT steps, respectively, and $(1, 3)$ the concerted pathway.⁴³ The free energy curves along the solvent coordinate, $G_i(\Delta E_{ij})$, are generated by the MC sampling described above, together with a free energy perturbation method⁴⁴ which allows the access to the thermally improbable regions of higher free energy. The solvation effects from outside of the spherical truncation are evaluated by using the reaction field approximation. The simulation uncertainty in the computed free energy curves is estimated to be ± 0.3 kcal/mol.

The basic strategy, given the above, can now be described, for simplicity, in the context of the first PT step of Scheme 1. The solvent coordinate and associated free energy calculations are used to access important solvent configurations associated with the reaction, e.g., those associated with the crossing of the diabatic free energy curves. Those solvent coordinate locations provide solvent molecule configurations in which the electronically adiabatic proton potential curves, as a function of the proton coordinate, are computed at a CI level (the CI(SD)/6-31G**-(F+) level calculations mentioned above). This is done for a variety of solvent molecule configurations at a given value of the solvent coordinate ΔE , and then the process is repeated at other values of the ΔE coordinate.⁴⁵ For each proton potential curve obtained, the proton vibrational motion is quantized by solution of a nuclear Schrödinger equation, to provide the ground (and first excited) proton vibrational level. The latter energy in the presence of the solvent (orientational) polarization as a function of the solvent coordinate then provides the overall free energy profile for the reaction step. It is important to note that the process just described calculates the electronically adiabatic proton potential energy curves; in that context, the diabatic perspective based solvent coordinate and associated preliminary free energies are devices employed to access interesting and important solvent configurations for which to perform the electronic adiabatic calculations.

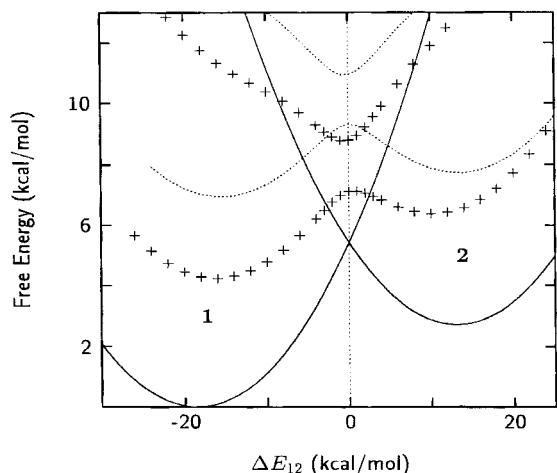


Figure 1. Diabatic free energy curves in the solvent coordinate ΔE_{12} , with the lowest two proton vibrational levels (including the solvent self-free-energy) (+++). These latter govern the adiabatic PT reaction. The F–O and O–O distances are 2.57 and 2.83 Å. The thin dotted line denotes the adiabatic proton levels at shorter O–O distance of 2.56 Å. The significance of these two O–O distance choices is discussed in text.

3. Stepwise Pathway

Here we describe the results for the first and second PT steps under the stepwise assumption for the double PT in Scheme 1. This stepwise choice is later justified in section 4.

3.1. First Proton Transfer Step. Figure 1 shows the calculated free energy curves in the solvent coordinate ΔE_{12} for the first PT step $1 \rightarrow 2$ producing the contact ion pair. The F–O and O–O distances are 2.57 and 2.83 Å, respectively. The reorganization energy⁴⁶ from the diabatic free energy curves (solid) in the figure is computed to be 15.8 kcal/mol, which indicates that the equilibrium solvation states for **1** and **2** are well separated in the solvent polarization coordinate. Further, it is already seen from the diabatic curves that the ionization process is endothermic, $\Delta G_{12} > 0$, and there exists an activation barrier ΔG_{12}^\ddagger in the solvent coordinate. The precise values of these quantities are determined in combination with the proton vibrational energy levels (cross marks in Figure 1), which will be explained presently. But at this point it is worth stressing again that the precise values referred to involve fully electronically adiabatic calculations for the proton potential; the present diabatic state calculations merely serve as a guide to locate important points in the solvent coordinate at which to perform those proton potential calculations, now discussed.

Figure 2 displays the calculated (CI(SD); cf. section 2) electronically adiabatic proton potential curves along the proton displacement coordinate r_1 , computed with the solvent configurations corresponding to the reactant, the diabatic crossing, and the product regions of the solvent coordinate ΔE_{12} . The solvent configurations at the given solvent coordinate values are sampled in the course of the Monte Carlo simulations, the methodological details of which have been described in ref 11 (see also section 2).

The evolving deformation pattern (asymmetric favoring reactants, symmetric, asymmetric favoring products) of the proton potentials seen in Figure 2a–c as a function of the solvent coordinate is in accordance with the postulated scheme of the proton potential modulation coupled to the solvent polarization fluctuation sketched in the Introduction. The lowest vibrational levels of the transferring proton, which are evaluated by numerically solving a one-dimensional Schrödinger equation for the proton motion, are also included in the figures, and are

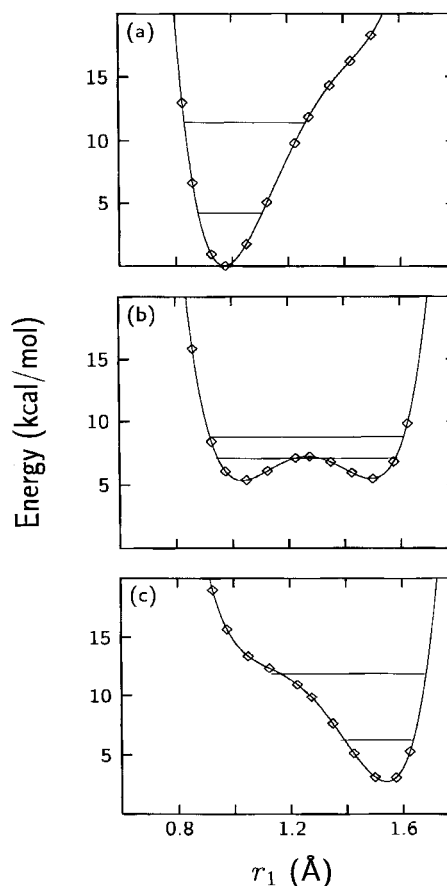


Figure 2. Proton transfer potentials, with the F···O distance at 2.57 Å, evaluated at negative, zero, and positive ΔE_{12} values. The ground and first excited proton vibrational levels are displayed. The marks are the computed points, and the curves are obtained by spline interpolation.

consistent with adiabatic PT. In particular, it is seen that the splitting of the ground and the first excited proton levels at the transition state $\Delta E_{12} = 0$ in Figure 2b is as large as 1.7 kcal/mol, and the ground level, i.e., the protonic zero-point energy, lies only slightly below the proton barrier top; this is a manifest signature of an adiabatic (nontunneling) PT mechanism.

Before proceeding to the presentation of the final free energy values for the first transfer, we pause to address an important issue. Since the solvent polarization is represented here by a one-dimensional solvent coordinate ΔE_{12} , there are many solvent configurations that give the same ΔE_{12} value. A question that must be considered is whether the proton potential barrier height may vary due to different solvent samplings at fixed ΔE_{12} , which if it were the case, would indicate that ΔE_{12} is insufficient as a reaction coordinate. We have examined this issue for the symmetric curve in Figure 2b at $\Delta E_{12} = 0$, since it is most relevant for the proton adiabaticity argument, and have found that the variance of the proton barrier height is 0.07 kcal/mol from 100 independent configuration samplings separated by at least 5×10^5 Monte Carlo steps; the influence on the zero-point proton vibrational level will be even smaller. Moreover, when we average out the small asymmetries by taking the mean value of the barrier heights in forward and backward PT directions, the variance is further reduced to 0.004 kcal/mol. That this variance is so small can be understood by the following considerations: The ΔE_{12} coordinate is most closely (or directly) connected to the energy difference between the two points of the proton coordinate corresponding to the minima of the potential curves in Figure 2. When this difference is fixed, for

example, at $\Delta E_{12} = 0$, the shape of the proton potential is primarily determined by other factors, not very sensitive to the different samplings, such as the inherent bond strengths of HF and OH (or the proton affinities of F^- and H_2O), the hydrogen-bonding distance and strength, the electronic coupling between the covalent and ionic VB states, and so on. In consequence, and as observed, the proton potential is not very much affected by different samplings at fixed ΔE_{12} , and the solvent polarization is indeed identified to be well characterized by this ΔE coordinate.⁴⁷

Returning to the main thread, the small cross marks in Figure 1 combine the free energy curves and the proton vibrational levels in Figure 2, which provides the final free energetics of the simulated system.⁴⁸ From these, the free energies of activation ΔG_{12}^\ddagger and reaction ΔG_{12}^0 are computed to be 2.9 and 2.2 kcal/mol, respectively.⁴⁹ The simulation uncertainty is estimated to be about 0.3 kcal/mol for the calculation of ΔG_{12}^0 (and yet smaller for ΔG_{12}^\ddagger). The root-mean-square (rms) deviation of the fitting of the Monte Carlo data points to the parabolic free energy curves in Figure 1 is about 0.9 kcal/mol.

The transition state location for the full free energy curve including the proton zero point motion is shifted to the right of $\Delta E_{12} = 0$, toward the contact ion pair product. This type of behavior, which is consistent with the Hammond postulate,⁵⁰ was found in the (appropriately) opposite direction for HCl both in aqueous solution¹¹ and at the ice surface.²³ Such behavior follows from a general analytical model of adiabatic PT reactions.⁵¹

The proton adiabatic transfer mechanism just found will be examined from a different perspective in section 3.4, but at this stage, there are several other aspects to mention that lend further support to the proton adiabatic mechanism. One is a possibility of pathways via attainment of shorter F–O distances, realized by its thermal fluctuation, and the other is the solvent electronic polarization effects that are treated only in an effective way⁵² in the present simulation. As has been discussed extensively in ref 11 for HCl ionization, both of these features tend to lower the proton potential barrier at the crossing point, such as to make the PT even more adiabatic, and we anticipate that this would also apply for HF. Finally, one might wonder about the influence of the compression of the O_a – O_b to 2.56 Å (the equilibrium distance for H_3O^+ – H_2O in $H_9O_4^+$ cluster) on the process. Calculation shows that such a compression has a free energy cost of 2.7 kcal/mol in the reactant state **1**. As a consequence, the associated free energy barrier is also higher for this route, while on the other hand the proton potentials are not much affected.

Figure 3 shows energetic and configurational distributions of a water molecule in the vicinity of the oxygen lone pair (that is not involved in the hydrogen bonding to HF) of the proton-accepting water in the first PT step. We note that they are sampled in the MC simulation of the solution system, so that the interactions and correlations with the other solvent molecules are fully taken into consideration. As seen, a linear hydrogen bonding is formed between this specific water and the proton-accepting water in the reactant state **1**, which is broken in the product state **2** to form a charge–dipole type configuration. In the transition state $\Delta E_{12} = 0$, the configuration is intermediate. These observations thus strongly suggest that the flipping motion of that specific water molecule, as illustrated in Figure 3d, plays a significant role in promoting the PT reaction. These types of motion were first seen in the HCl ionization case^{10,11} and were later proposed in connection with proton transport in water by

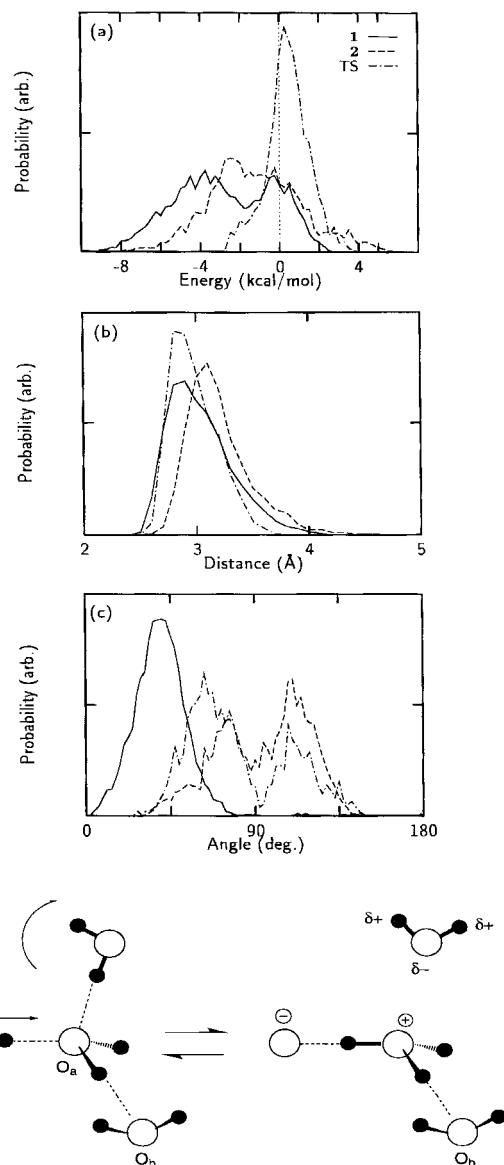


Figure 3. Energetic and configurational distributions of a water molecule in the vicinity of the oxygen lone pair (that is not involved in the hydrogen bonding to HF) of the proton-accepting water in the first PT step: (a) the H_2O – H_2O_a (or $H_3O_a^+$) interaction energy, (b) the O – O_a distance, and (c) the angle between the O – O_a direction and the external water molecule's dipole direction. Solid, dot, and dash-dot lines correspond to the reactant **1**, the product **2**, and the transition state $\Delta E_{12} = 0$, respectively. (d) Schematic illustration of the possible reaction-promoting motion suggested from the distribution results.

Agmon;⁵³ Something very similar was in fact suggested long ago by Newton.⁵⁴

3.2. Mulliken Charge Transfer Picture. The character of the evolving charge distributions of the reaction participants for the first PT step is of considerable interest in connection with the unconventional Mulliken charge transfer picture for PT reactions.^{25,26} In this picture, the electronic character of the process consists of charge transfer from a nonbonding (lone pair) orbital of the base, here H_2O , to an antibonding orbital of the acid, here HF. This weakens the HA bond and a species somewhat akin to an H atom is transferred. (In simple VB language, the two electronic structures involved are just the two VB states that we have referred to throughout.) This view has been supported in our previous investigation of HCl acid ionization,¹¹ and we investigate its applicability here, stressing again that the electronic structure calculations determining the

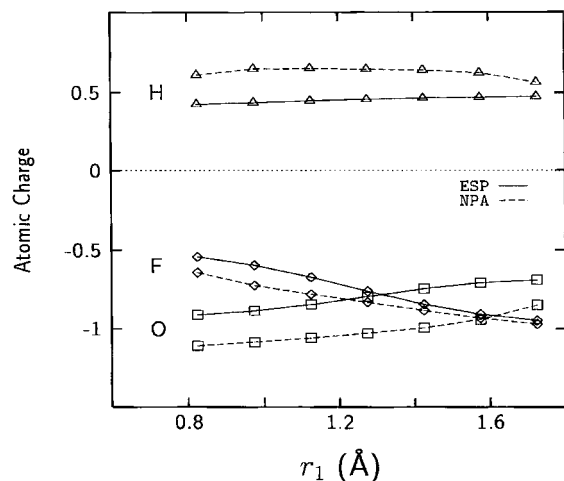


Figure 4. Atomic charges variation along r_1 of F, O_a, and transferring H, derived from the electrostatic potential (ESP, solid) and from the natural population analysis (NPA, dashed), using MOs at $\Delta E_{12} = 0$.

TABLE 3: NBO Occupations of F–H Bonding and Antibonding (F–H*) Orbitals and Oxygen Lone Pair (lp) Orbital in the F–H···O Direction^a

r_1 (Å)	F–H	F–H*	O (lp)	H (tr)
0.925	1.9998	0.0573	1.9367	0.6380
0.975	1.9998	0.0731	1.9210	0.6454
1.000	1.9998	0.0815	1.9127	0.6475
1.100	1.9997	0.1175	1.8776	0.6487
1.200	1.9997	0.1558	1.8400	0.6450

^a The rightmost column shows the natural population on the transferring proton.

charges to be discussed are electronically adiabatic, determined via MO calculations (at RHF level), without any reference at all to a simple two VB state composition.

We choose to examine the charges on the O atom of the water base, on the F atom of the acid, and the transferring hydrogen species via the device of simply determining, by least-squares fitting, the charges necessary to reproduce the electrostatic potential around the immersed solute pair. This is done in the presence of the surrounding water molecules for $\Delta E_{12} = 0$, corresponding to the transition state identified above, and as a function of the proton coordinate. The results are shown in Figure 4, where the charge transfer character is clearly apparent. The charge on the hydrogenic species is essentially constant and less than 0.5. The smooth reduction of the negative charge on the basic O moiety and the corresponding smooth increase in the negative charge magnitude of the F moiety completes the picture. Basically, the same picture emerges from the “natural population analysis⁵⁵” shown by the dashed lines in Figure 4.

Table 3 lists the occupancy of the “natural bond orbitals (NBOs)⁵⁵” corresponding to the F–H bonding and antibonding orbitals, and the oxygen lone-pair orbital in the FH···O direction, as functions of the proton coordinate r_1 , computed from the RHF MOs at the transition state $\Delta E_{12} = 0$. The natural population on the transferring proton discussed above is also listed. As seen, the PT is clearly correlated to the charge transfer from the oxygen lone pair to the F–H antibond while the occupation of the F–H bond orbital and the population on the transferring proton remain nearly constant.⁵⁶

3.3. Second Proton Transfer Step. We now turn to the second step of the ionization in Scheme 1, in which the hydronium ion in the contact ion pair produced by the first step transfers a proton to a neighboring water molecule to produce

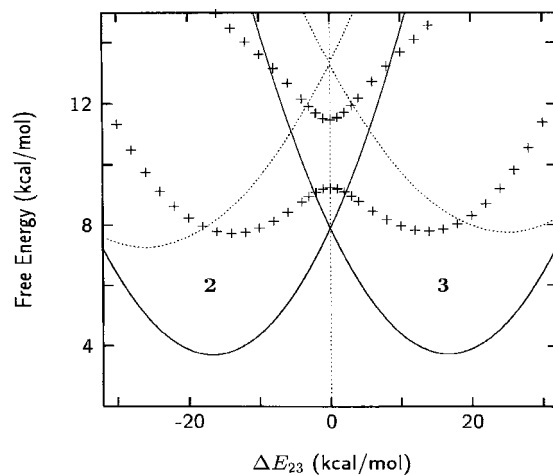


Figure 5. Same as Figure 1, but for the 2 → 3 second PT step. The solvent coordinate is ΔE_{23} , and the O–O distance is 2.56 Å. The thin dotted lines are the adiabatic curves at larger O–O distance of 2.83 Å.

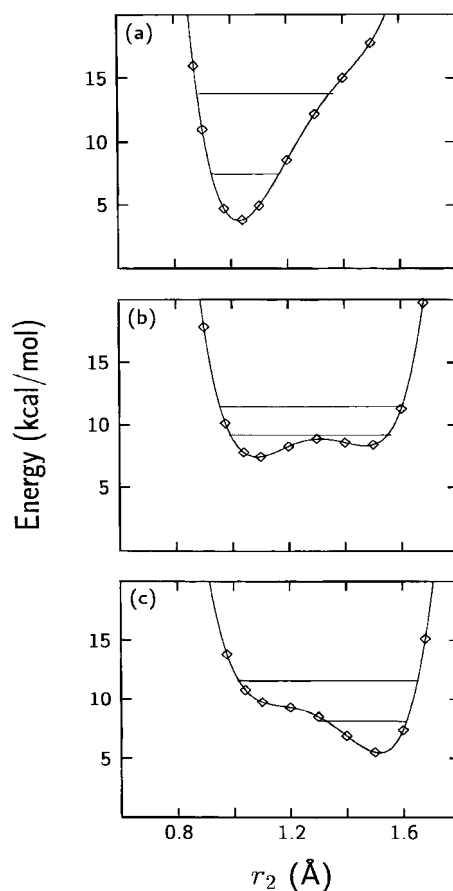


Figure 6. Same as Figure 2, but for the second PT step 2 → 3.

a solvent-separated ion pair. Here we treat this step as consecutive compared to the first PT step, rather than as concerted with it; this approach is supported below.

Figures 5 and 6 display the corresponding solvent free energy curves and proton transfer potentials calculated for the second PT 2 → 3 in the solvent coordinate ΔE_{23} . The O–O distance R_{OO} is taken to be 2.56, which is the equilibrium distance between H_3O^+ and H_2O in the $\text{H}_3\text{O}^+(\text{H}_2\text{O})_3$ cluster. Indeed, this separation is slightly less stable in free energy in solution than the H_2O – H_2O equilibrium value of 2.83 (from the $(\text{H}_2\text{O})_5$ cluster), although the difference is almost within the simulation uncertainty. As discussed previously, the stabilization of the larger O–O distance in solution compared to the situation in a

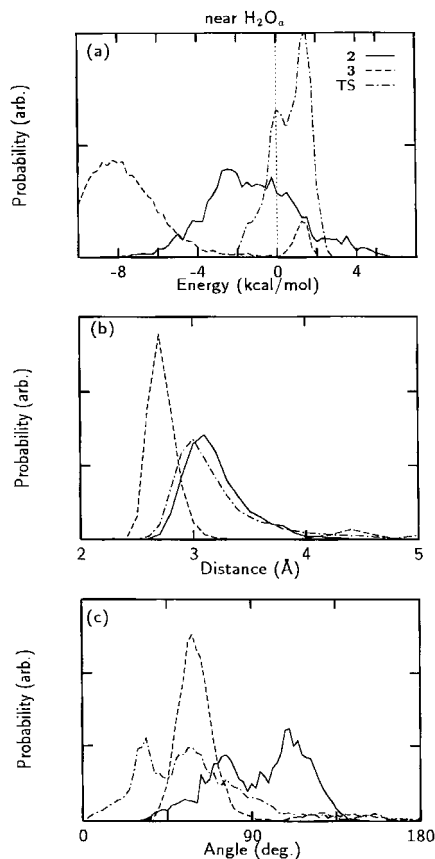


Figure 7. Same as Figure 3, but for the second PT step.

hydrated cluster might reflect the influence of the bulk polar water solvent favoring a larger $\text{H}_3\text{O}^+ - \text{H}_2\text{O}$ separation associated with a more localized charge distribution. On the other hand, the activation barrier to the transition state is apparently smaller for the shorter O—O distance (primarily due to the smaller reorganization energy).

It is seen in Figure 6 that the second PT is proton adiabatic: the ground proton vibrational level is above the proton barrier in Figure 6b. The free energy curves in Figure 5 show that this second transfer is nearly thermodynamically neutral, with an estimated reaction free energy (taking account of the quantized proton levels) of ΔG_{23}^0 of only -0.1 kcal/mol. However, activation in the solvent is required for this PT step to occur, for which the activation energy is estimated to be $\Delta G_{23}^\ddagger = 1.5$ kcal/mol. The solvent reorganization energy is 16.7 kcal/mol, so that the states **2** and **3** are well separated in the solvent coordinate.⁵⁷

We see in Figures 5 and 6 that the postulated scheme described in the Introduction is appropriate also for the second PT between H_3O^+ and H_2O . However, the reaction is not usefully regarded in covalent versus ionic terms (as for the first PT) but rather is similar to a (symmetric) charge-shift reaction, since the proton affinities of the two proton sites are almost the same. We take a perspective that the polar aqueous solvation prefers the excess proton localized within the asymmetric proton potential wells around either of the H_3O^+ sites in the equilibrium reactant or product states.⁵⁸ Activation in the solvent coordinate is required to reach the transition state between the two equilibrium states, at which the proton potential is symmetric.

Figures 7 and 8 shows the distribution functions of water molecules in the vicinity of H_2O_a and H_2O_b , respectively. A picture that emerges from these results is basically the same as that discussed in ref 11 for HCl ionization: the water molecule

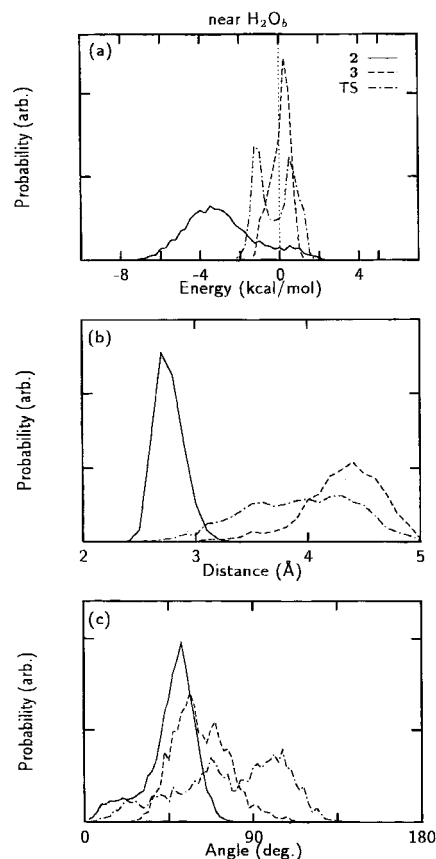


Figure 8. Same as Figure 7, but for a water in the vicinity of H_2O_b which is the accepting proton in the second PT step.

TABLE 4: Landau–Zener Parameters^a

step R_{OO} (Å)	1 \rightarrow 2		2 \rightarrow 3	
	2.83	2.56	2.83	2.56
λ (kcal/mol)	15.8	16.8	27.1	16.7
C (kcal/mol)	0.84	0.82	0.04	1.12
P_{LZ}	0.59	0.56	1.7×10^{-3}	0.79
$2P_{\text{LZ}}/(1 + P_{\text{LZ}})$	0.74	0.72	3.5×10^{-3}	0.88

^a The characteristic frequency of the solvent coordinate motion is taken to be 400 cm^{-1} .

hydrogen bonded to H_2O_b in state **2** turns away from H_3O_b^+ in state **3**, and the water in the vicinity of H_3O_a^+ in state **2** that has turned away in the first PT step as described in section 3.1 comes back to hydrogen bonding to neutral H_2O_a , in state **3** (see Figure 12 of ref 11).

3.4. Adiabaticity from a Curve-Crossing Model. A more detailed examination of the proton adiabaticity can be undertaken. In Table 4 we summarize the Landau–Zener transition probability P_{LZ} and the net transmission probability $P \equiv 2P_{\text{LZ}}/(1 + P_{\text{LZ}})$ which measure the adiabaticity of PTs on the basis of a dynamical curve-crossing model.⁷ We refer again to ref 11 for details.

For the plausible stepwise pathway discussed above, **1** \rightarrow **2** at $R_{\text{OO}} = 2.8 \text{ Å}$ and **2** \rightarrow **3** at $R_{\text{OO}} = 2.6 \text{ Å}$, the adiabaticity parameter P is close to but slightly smaller than unity, 0.74 and 0.88, indicating there are small dynamical nonadiabatic effects at the current level of treatment. However, as discussed extensively in ref 11 (and mentioned briefly in section 3.1), there is an assortment of possibilities that may further increase the adiabaticity on going beyond the present modeling, such as pathways via shorter F—O distance and the solvent electronic polarization effects. Having these in mind, we anticipate that

both the first and second PT steps of HF ionization are almost fully adiabatic, though this could and should be examined at a higher level in the future.

4. Consecutive versus Concerted Pathway, HF Acid Weakness, and IR-Induced Dissociation

4.1. Consecutive versus Concerted Pathway. Here we examine the issue of stepwise versus concerted PT in Scheme 1 by calculation of the free energy curves for the concerted double transfer, in order to support our choice of the stepwise pathway. The activation energy to reach the transition state for the concerted double transfer, computed from the diabatic⁵⁹ free energy curves in the solvent coordinate ΔE_{13} , is 10.6 kcal/mol, which is significantly larger compared to those for the stepwise transfers. As discussed in ref 11, this can be comprehended from the larger solvent reorganization⁶⁰ associated with the larger charge separation for $\mathbf{1} \rightarrow \mathbf{3}$. In ref 11, we also argued (for the case of HCl ionization) that there are in fact three more biases against the concerted pathway: (1) there exists a large proton potential barrier along the second proton coordinate r_2 at the diabatic crossing $\Delta E_{13} = 0$ for the O–O separation of 2.83 Å; (2) compressing the O–O distance decreases the proton barrier, but involves a significant free energy cost, particularly in the reactant state $\mathbf{1}$; (3) even at the diabatic crossing ΔE_{13} , simultaneous double PT (i.e., the diagonal direction on the proton potential $V(r_1, r_2)$) is unfavorable (for both $R_{OO} = 2.83$ and 2.56 Å), because the energy cost of the two bond breaking is not compensated by the gain by solvation, due to the charge delocalized nature of intermediate structure (at the middle of the diagonal path). These assorted penalties also apply for the HF ionization considered here, and we conclude again that the concerted pathway for the double PT in Scheme 1 is unfavorable compared to the stepwise one. We anticipate that the qualitative arguments here would also apply for general proton transport processes in water, which is in contrast with e.g. a previously suggested solitonic mechanism.⁶

4.2. HF Acid Weakness. With the consecutive two-step pathway established, we can turn to the issue of the HF weak acid character in aqueous solution raised in the Introduction. First, to place things in perspective, we need to connect the current estimates of the reaction free energies to the ΔG^0 value for the reaction in bulk to produce free ions. The experimental pK_a of HF in water is ca. +3, which corresponds to $\Delta G_{12} \approx +4$ kcal/mol. The present calculations show that the reaction free energy for the first PT step is $\Delta G_{12} = 2.2$ kcal/mol, and the second PT step is almost thermoneutral within the simulation uncertainty. The calculations thus indicate that the overall small acid strength of HF in water is already largely reflected in the very first step to produce the contact ion pair. This contrasts with the alternate scenario advocated¹⁷ in which that step is thermodynamically favorable, with the weak acid character arising instead from the high cost of separating the contact ion pair into free ions.⁶²

From a simple screened Coulomb argument, the free energy cost to separate the ion pair in state $\mathbf{3}$, with F–O_b distance of 4.4 Å, to infinite separation is estimated to be 0.95 kcal/mol with the use of the dielectric constant of water ($\epsilon = 79$). (The same argument gives 1.63 kcal/mol for the separation from the contact ion pair $\mathbf{2}$. The small difference between these two values (~ 0.7 kcal/mol) would be another qualitative support for the small reaction free energy obtained for the second PT step.) Given the resultant small reaction free energy of the second PT step (which is also supported by the dielectric screening argument), and the expected thermoneutrality of the

rest of the ion separation process that should be more or less similar to the bulk proton conduction, it would be reasonable to consider that the overall endothermicity of the HF ionization is achieved by the first PT step. On the other hand, considering that even the most elaborate quantum chemical calculations cannot predict decided accuracy of kcal/mol, and that we introduced many approximations in the modeling of the complex solution phase system, we do not absolutely rule out possibility that some fraction of the endothermicity could come from the second step (and from the next PT step to produce the “contact hydrated complexes”—see also section 5).

4.3. IR-Induced Dissociation. The possibility that PT reactions in solution might be induced by vibrational excitation of the proton stretch has received some discussion^{63,64} and the basic picture for how this would proceed in an acid–base adiabatic PT reaction has been described.⁶⁴ The reader is referred in particular to ref 64, which forms the background for the present discussion. Figure 1 for the first PT step displays the full free energies, including the energies for the ground $\nu = 0$ and first excited $\nu = 1$ proton vibrational states, which we now label as G_0 and G_1 , versus the solvent coordinate. Inspection of this figure shows that on vibrational excitation $\nu = 0 \rightarrow \nu = 1$ of the undissociated HF, the Franck–Condon transition places the system at an unstable point on the upper curve G_1 . The solvent will then relax to the bottom of this free energy curve, the proton remaining in its excited vibrational state. An ensuing nonadiabatic transition from the region of the minimum to G_1 to the ground state surface G_0 , which corresponds to vibrational deexcitation of the proton, places the system in the region of the G_0 surface transition state. From here, solvent motion can produce the product contact ion pair (as well as the original reactant pair). In this process, by which the ground state barrier has in effect been circumvented by vibrational excitation, attention needs to be paid⁶⁴ to the role of the F···O hydrogen bond vibration, which is involved in determining the vibrational deactivation rate, for a full description, to be addressed elsewhere. In addition, the present estimate of a small barrier (0.8 kcal/mol, see section 5) for the collapse of the contact ion pair should be examined in more detailed calculations to confirm that a well-defined product state actually exists. Nonetheless, the present discussion based on the computed free energy curves of Figure 1 indicates that the aqueous HF system might provide an interesting possibility for vibrational photochemistry in solution.

5. Recombination Process

In the preceding sections, we examined the mechanism of HF ionization in water in terms of the free energetics. On the basis of these results, we can now discuss aspects of the reverse process, i.e., the ion recombination reaction of $F^-/H_3O^+(aq)$ to form HF(aq). Indeed, because HF is a weak acid ($pK_a \approx +3$), the recombination process is more accessible by standard kinetic experiments.

The free energy curves in Figures 1 and 5 (for the stepwise pathway) indicate that the final steps of the ion recombination $\mathbf{3} \rightarrow \mathbf{2} \rightarrow \mathbf{1}$ proceed by going down an “free energy funnel”, but by surmounting activation barriers in the solvent coordinate along the way. The computed free energy barriers for the steps $\mathbf{3} \rightarrow \mathbf{2}$ and $\mathbf{2} \rightarrow \mathbf{1}$ are $\Delta G_{32}^\ddagger = 1.6$ kcal/mol and $\Delta G_{21}^\ddagger = 0.8$ kcal/mol, respectively, so that the barrier height decreases as the ions approach each other. This is the key insight concerning the recombination process that results from the present study. We now attempt to put this into perspective for the overall recombination process.

Kinetic experiments have provided the activation energies for proton conduction in bulk water and for the (overall) ion recombination $\text{OH}^- + \text{H}^+ \rightarrow \text{H}_2\text{O}$ to be 2.4 and 3 kcal/mol, respectively.^{4,65} The combination of these numbers with our estimates for the energy funnel steps above would indicate that the entire ion recombination of $\text{F}^- + \text{H}_3\text{O}^+ \rightarrow \text{HF}$ is limited by encounter of the ions at a separation certainly larger than that appropriate for the contact pair, and that the production of that encounter involves the Grotthuss transport of the proton.

Eigen et al. analyzed⁴ the experimental relaxation time associated with the equilibrium $\text{OH}^- + \text{H}^+ \rightleftharpoons \text{H}_2\text{O}$ in pure water to yield the overall rate constants of the recombination and dissociation reactions. By employing a Debye-type diffusion-limited encounter model, they derived a "reaction distance" of the ion recombination to be 8 Å. Since 8 Å corresponds to the cross sections of hydrated complexes H_9O_4^+ and H_7O_4^- , they proposed a picture⁴ that "instantaneous charge neutralization occurs as soon as the two complexes are bridged by at least one hydrogen bond." Here we apply their analysis for $\text{F}^- + \text{H}_3\text{O}^+ \rightarrow \text{HF}$ by using their kinetic experimental data⁶⁶ and obtain the recombination distance of 8.2 Å, which would be interpreted as a contact separation of the hydrated complexes $\text{F}^- (\text{H}_2\text{O})_4$ and $\text{H}_3\text{O}^+(\text{H}_2\text{O})_3$. This situation of contact complexes corresponds to, say, a state **4** that is to be formed by proceeding one ionization step in the forward direction beyond the solvent-separated ion pair **3** in Scheme 1. Although we have not carried out calculations on this PT process **3** \rightarrow **4**, it could be reasonably assumed to be similar to our second PT step **2** \rightarrow **3**, i.e., an adiabatic PT at O–O distance of ~ 2.6 Å; this step should be nearly thermoneutral (since the influence of the more distantly located F^- ion on the reaction free energy is expected to be smaller, due to more effective dielectric screening) with a solvent barrier of about ~ 2 kcal/mol (alternately, the barrier might be viewed as something between those for the **2** \rightarrow **3** step and bulk proton transport). Unfortunately, there is enough uncertainty in the estimates for the barrier of this **4** \rightarrow **3** step to preclude any clear statement as to whether the approach to state **4** or to state **3** is rate-limiting. With this proviso then, the picture that emerges is that the ion recombination of $\text{F}^- + \text{H}_3\text{O}^+$ is limited by an encounter, whose generation involves Grotthuss transport of the proton, in which is formed either the contact hydration complexes (**4**) or the solvent-separated ion pair (**3**), and the transformation thereafter (**4** \rightarrow **3** \rightarrow **2** \rightarrow **1**) occurs rapidly by transit down the free energy funnel with small solvent barriers.

6. Concluding Remarks

In this work we have examined, by a combination of electronic structure and Monte Carlo methodologies, the first two steps of the acid ionization of HF in aqueous solution.

The picture that emerged for these steps is that of consecutive adiabatic (nontunneling) and stepwise PTs. With the important difference that the first step for the HF ionization is uphill in free energy and for HCl is downhill,¹¹ the overall microscopic character of the HF ionization steps are quite similar to those of its HCl cousin.

The endothermicity in free energy terms of the overall HF ionization is largely associated with the first PT step **1** \rightarrow **2** to produce the contact ion pair. This contrasts with a suggestion that such a step would be strongly thermodynamically favored and that the weakness of HF acid would arise from an unfavorable separation of the ions. Our calculation indicates that HF is a weak acid because the (internal) energy cost (or the proton affinity difference) to produce the contact ion pair is larger than the energy stabilization gain by the ion pair solvation (whereas for HCl, the latter is larger.)

Concerning other aspects of the reaction, the proton adiabatic character of the contact ion pair producing first step was used to examine, in a preliminary way, the potential of this reaction for being accelerated by proton excitation, as a possible candidate for mode-selective chemistry in solution. In addition, the charge distribution variations associated with the first PT step were found to support, as was the case for HCl ionization,¹¹ the Mulliken view of the electronic character of PT reactions.⁶⁷

The ion recombination process was found (perforce) to also be adiabatic and stepwise, and adds a picture of a final recombination stage involving an energy funnel with small barriers in several steps to the well-known picture of the recombination process due to Eigen.

Acknowledgment. K.A. acknowledges support from University of Tsukuba Research Projects and Grants in Aid for Scientific Research from the Ministry of Education (Nos. 09740415 and 10120203). J.T.H. acknowledges support via NSF grant CHE 9700419. This paper was completed while J.T.H. was a visiting Condorcet Professor in the Département de Chimie, Ecole Normale Supérieure, Paris. Useful discussions with Dr. Thomas Schroeder are acknowledged. J.T.H. takes this opportunity to express his keen appreciation for the pleasure of his past collaborations with Kent Wilson, and even more importantly, his deep admiration for Kent's enthusiastic, idiosyncratic, and courageous approach to discovering nature's wonders.

Appendix

Here we describe an interpolation method to construct continuous deformation of the proton potential curves as a function of the solvent coordinate, which is needed for calculation of the adiabatic proton levels (cross marks) in Figures 1 and 5.

To be concrete, we consider the first PT step and denote the curves in Figure 2a–c by $V_1(r)$, $V_0(r)$, and $V_2(r)$, respectively. In addition, r_i and r_f are defined by the proton coordinate values corresponding to the two minima in $V_0(r)$. Then, we describe the deformation of the proton curve as a function of the solvent coordinate ΔE_{12} (in the region of $\Delta E_{12} \leq 0$) by

$$V(r, \Delta E_{12}) = V_1(r) + \frac{\Delta E_{12} - \Delta V_1}{\Delta V_1 - \Delta V_0} (V_1(r) - V_0(r))$$

in which $\Delta V_I \equiv V_I(r_i) - V_I(r_f)$ for $I = 0, 1$, and 2. In $\Delta E_{12} > 0$ region, we replace $V_1(r)$ and ΔV_1 in above by $V_2(r)$ and ΔV_2 . By this, the following relation is always satisfied:

$$V(r_i, \Delta E_{12}) - V(r_f, \Delta E_{12}) = \Delta E_{12}$$

In particular, this means $V(r_i, 0) = V(r_f, 0)$; i.e., the proton curve is "symmetric" at $\Delta E_{12} = 0$. The same procedure is straightforwardly applied to the second PT step.

References and Notes

- (1) Bell, R. P. *The Proton in Chemistry*; Chapman and Hall: London, 1973. Caldin, E. F., Gold, V., Eds. *Proton Transfer Reactions*; Chapman and Hall: London, 1975. Bell, R. P. *The Tunnel Effect in Chemistry*; Chapman and Hall: London, 1980. Bunce, E., Lee, C. C., Eds. *Isotope Effects in Organic Chemistry*; Elsevier: Amsterdam, Vol. 2, 1976; Hibbert, F. *Adv. Phys. Org. Chem.* **1986**, 22, 113. Hibbert, F. *Adv. Phys. Org. Chem.* **1990**, 26, 255. Westheimer, F. H. *Chem. Rev.* **1961**, 61, 265.
- (2) (a) Kosower, E. M.; Huppert, D. *Annu. Rev. Phys. Chem.* **1986**, 37, 127. Kreevoy, M. M.; Truhlar, D. G. In *Rates and Mechanisms of Reactions*, 4th ed.; Bernasconi, C. F., Ed.; Wiley: New York, 1986, Chapter 1. Ratajczak, H. In *Electron and Proton Transfer Processes in Chemistry and Biology*; Müller, A., Ratajczak, H., Junge, W., Diemann, E., Eds.;

- Elsevier: Amsterdam, 1992. (b) Bountis, T., Ed. *Proton Transfer in Hydrogen-Bonded Systems*; Plenum: New York, 1993. (c) See also the special issues on proton transfer: *Chem. Phys.* **1989**, *136*, 2; *J. Phys. Chem.* **1991**, *95*, 25, and *Ber. Bunsenges. Phys. Chem.* **1998**, *102*, 3.
- (3) Jencks, W. P. *Catalysis in Chemistry and Enzymology*; McGraw-Hill: New York, 1969. Bender, M. L. *Mechanisms of Homogeneous Catalysis from Protons to Proteins*; Wiley: New York, 1971. Fersht, A. *Enzyme Structure and Mechanism*; W. H. Freeman: New York, 1985; Gandour, R. D.; Schowen, R. L. *Transition States of Biochemical Processes*; Plenum: New York, 1978. Klinman, J. P. *CRC Crit. Rev. Biochem.* **1981**, *10*, 39. Menger, F. *Acc. Chem. Res.* **1993**, *26*, 206. Gutman, M.; Nachliel, E. *Biochim. Biophys. Acta.* **1990**, *391*, 1015.
- (4) Eigen, M.; Kruse, W.; De Maeyer, L. *Prog. React. Kinet.* **1964**, *2*, 285. Eigen, M. *Angew. Chem., Int. Ed. Engl.* **1964**, *3*, 1; *Pure Appl. Chem.* **1963**, *6*, 97.
- (5) Albery, W. J. *Prog. React. Kinet.* **1967**, *4*, 353. Maxrchal, Y. In ref 2b.
- (6) Borgis, D.; Lee, S.; Hynes, J. T. *Chem. Phys. Lett.* **1989**, *162*, 19. Borgis, D.; Hynes, J. T. *J. Chem. Phys.* **1991**, *94*, 3619; *Chem. Phys.* **1993**, *170*, 315.
- (7) Borgis, D.; Hynes, J. T. *J. Phys. Chem.* **1996**, *100*, 1118.
- (8) Juanós i Timoneda, J.; Hynes, J. T. *J. Phys. Chem.* **1991**, *95*, 10431.
- (9) Staib, A.; Borgis, D.; Hynes, J. T. *J. Chem. Phys.* **1995**, *102*, 2487.
- (10) Ando, K.; Hynes, J. T. In Cramer, C. J.; Truhlar, D. G., Eds.; *Structure and Reactivity in Aqueous Solution: Characterization of Chemical and Biological Systems*; ACS Books: Washington DC, 1994. *J. Mol. Liq.* **1995**, *64*, 25.
- (11) Ando, K.; Hynes, J. T. *J. Phys. Chem. B* **1997**, *101*, 10464.
- (12) Ando, K.; Hynes, J. T. *Faraday Discuss.* **1995**, *102*, 435.
- (13) Ando, K.; Hynes, J. T. *Adv. Chem. Phys.* **1999**, *110*, 381.
- (14) Azzouz, H.; Borgis, D. *J. Chem. Phys.* **1993**, *98*, 7361; *J. Mol. Liq.* **1994**, *61*, 17. Borgis, D.; Tarjus, G.; Azzouz, H. *J. Phys. Chem.* **1992**, *96*, 3188; *J. Chem. Phys.* **1992**, *97*, 1390.
- (15) Warshel, A.; Weiss, R. M. *J. Phys. Chem.* **1980**, *102*, 6218. Warshel, A.; Russel, S. *J. Am. Chem. Soc.* **1986**, *108*, 6569. Warshel, A. *Computer Modeling of Chemical Reactions in Enzymes and Solutions*; Wiley: New York, 1991.
- (16) Laasonen, K.; Klein, M. L. *J. Am. Chem. Soc.* **1994**, *116*, 11620.
- (17) Giguere, P. A. *J. Chem. Ed.* **1979**, *56*, 571; *Chem. Phys.* **1981**, *60*, 421.
- (18) Laasonen, K.; Klein, M. L. *Mol. Phys.* **1996**, *88*, 135.
- (19) Balbuena, P. B.; Johnston, K. P.; Rossky, P. J. *J. Phys. Chem.* **1996**, *100*, 2716.
- (20) Kapral, R.; Consta, S. *J. Chem. Phys.* **1994**, *101*, 10908; **1996**, *104*, 4581. Laria, D.; Kapral, R.; Estrin, D.; Ciccotti, G. *J. Chem. Phys.* **1996**, *104*, 6560.
- (21) Chipot, C.; Gorb, L. G.; Rivail, J.-L. *J. Phys. Chem.* **1994**, *98*, 1601. Rivail, J.-L.; Antonczak, S.; Chipot, C.; Ruiz-López, M. F.; Gorb, L. G. In *Structure, Energetics, and Reactivity in Aqueous Solution*; Cramer, C. J., Truhlar, D. G., Eds.; ACS Books: Washington, DC, 1994.
- (22) Even if restricted to the theoretical arena, the general field of proton transfer research is now quite extensive. Some general sources of references here include refs 2 and 13, and the forthcoming special issues of *Isr. J. Chem.*, edited by N. Agmon and M. Gutman.
- (23) Gertner, B. J.; Hynes, J. T. *Science* **1996**, *271*, 1563. Gertner, B. J.; Hynes, J. T. *Faraday Discuss.* **1998**, *110*, 301. Bianco, R.; Gertner, B. J.; Hynes, J. T. *Ber. Bunsenges. Phys. Chem.* **1998**, *102*, 518. See also: Estrin, D. A.; Kohanoff, J.; Laria, D. H.; Weht, R. O. *Chem. Phys. Lett.* **1997**, *280*, 280.
- (24) Pauling, L. *The Nature of the Chemical Bond*; Cornell: Ithaca, NY, 1960. Coulson, C. A. *Valence*; Oxford: London, 1961.
- (25) Mulliken, R. S. *J. Phys. Chem.* **1952**, *56*, 801; *J. Chim. Phys.* **1964**, *20*, 20.
- (26) Coulson, C. A. In *Hydrogen Bonding*; Hadži, D., Thompson, H. W., Eds.; Pergamon: London, 1959. Szczepaniak, K.; Tramer, A. *J. Phys. Chem.* **1967**, *71*, 3035. Puranik, P. G.; Kumar, V. *Proc. Indian Acad. Sci.* **1963**, *29*, 58, 327. Zwilless, B. A.; Parson, W. B. *J. Chem. Phys.* **1983**, *79*, 65. Bacskay, G. B.; Hush, N. S. *Chem. Phys.* **1983**, *82*, 303. Reed, A. E.; Curtis, L. A.; Weinhold, F. *Chem. Rev.* **1988**, *88*, 899. See also refs 8 and 11.
- (27) See the discussion remarks following ref 12.
- (28) Marcus, R. A. *Annu. Rev. Phys. Chem.* **1964**, *15*, 155. Ulstrup, J. *Charge Transfer Processes in Condensed Media*; Springer-Verlag: Berlin, 1979. Newton, M. D.; Sutin, N. *Ibid.* **1984**, *35*, 437. Bagchi, B. *Annu. Rev. Phys. Chem.* **1989**, *40*, 115. Barbara, P. F.; Meyer, T. J.; Ratner, M. A. *J. Phys. Chem.* **1996**, *100*, 13148.
- (29) An entree into the extensive literature may be found in: Marx, D.; Tuckerman, M. E.; Hutter, J.; Parrinello, M. *Nature* **1999**, *397*, 601. Hynes, J. T. *Nature* **1999**, *397*, 565. See also refs 53 and 54 below.
- (30) See e.g.: Kierstead, W. P.; Wilson, K. R.; Hynes, J. T. *J. Chem. Phys.* **1991**, *95*, 5256, and references therein.
- (31) Dupuis, M.; Watts, J. D.; Villar, H. O.; Hurst, G. J. B. HONDO Ver. 7.0, *QCPE*, 1987, 544.
- (32) Spangler, D.; Williams, I. H.; Maggiora, G. J. *Comput. Chem.* **1983**, *4*, 524.
- (33) Binkley, J. S.; Pople, J. A.; Hehre, W. J. *J. Am. Chem. Soc.* **1980**, *102*, 939. Hehre, W. J.; Ditchfield, R.; Pople, J. A. *J. Chem. Phys.* **1972**, *56*, 2252.
- (34) Allen, M. P.; Tildesley, D. J. *Computer Simulation of Liquids*; Clarendon: Oxford, UK, 1987.
- (35) Shavitt, I. In *Methods of Electronic Structure Theory*; Schaefer, H. F., III, Ed.; Plenum: New York, 1977.
- (36) Dunning, T. H.; Hay, P. J. In *Methods of Electronic Structure Theory*; Schaefer, H. F., III, Ed.; Plenum: New York, 1977.
- (37) Langhoff, S. R.; Davidson, E. R. *Int. J. Quantum Chem.* **1974**, *8*, 61.
- (38) We also introduced an energy correction for the solute internal energy term in the model potential for the simulation, determined from calculation of proton potential curves for the HF \cdots H $_2$ O complex by larger CI(SD) in the "split-valence" CI space with no frozen core orbitals (10 electrons in 24 orbitals). The number of configuration state functions is 10011. As expected, this extensive account of the electron correlation effects stabilizes the covalent structure compared to the ionic one, which turns out to contribute essentially to the resultant endothermicity of the first PT step.
- (39) Jorgensen, W. L.; Chandrasekhar, J.; Madura, J.; Impey, R. W.; Klein, M. L. *J. Chem. Phys.* **1983**, *79*, 926.
- (40) Möller, C.; Plesset, M. S. *Phys. Rev.* **1934**, *45*, 618. Krishnan, R.; Frisch, M. J.; Pople, J. A. *J. Chem. Phys.* **1980**, *72*, 4244.
- (41) Clementi, E.; Barsotti, R. *Chem. Phys. Lett.* **1980**, *59*, 21. Mezei, M.; Beveridge, D. L. *J. Chem. Phys.* **1981**, *74*, 6902. Szasz, G. I.; Heinzinger, K. Z. *Naturforsch., A* **1979**, *34*, 840. Impey, R. W.; Madden, P. A.; McDonald, I. R. *J. Phys. Chem.* **1983**, *87*, 5071. Chandrasekhar, J.; Spellmeyer, D. C.; Jorgensen, W. L. *J. Am. Chem. Soc.* **1984**, *106*, 903.
- (42) The coordinates \mathbf{R}_i for states **2** and **3** are obtained by shifting the (transferring) two protons along the linear hydrogen bonds at distances $r(\text{HO}_a) = 0.975 \text{ \AA}$ (for **2** and **3**) and $r(\text{HO}_b) = 0.973 \text{ \AA}$ (for **3**). This simple procedure was taken because the contact ion pair state **2** is not stabilized in the small hydration cluster used in the present geometry optimization procedure. Much more elaborate (full quantum chemical) calculations on the systems **1–3** with at least eight (or more) solvating waters (see Figures 2 and 17 of ref 11) would be needed in order to optimize the structures of the ionic states **2** and **3**. However, these \mathbf{R}_i coordinates are used first for the determination of the charge parameters (Table 1) and then for the MC simulations, both of which would not be quite sensitive to the slight arbitrariness of the proton position.
- (43) The coordinates \mathbf{R}_i were fixed in the MC simulations. All of the three potentials V_i ($i = 1–3$) were computed at every MC step, one of which or a linear combination of the two is referred to for the Metropolis sampling test.
- (44) Ando, K.; Kato, S. *J. Chem. Phys.* **1991**, *95*, 5966.
- (45) We computed the potential energy surfaces as functions of the transferring two proton coordinates (r_1, r_2) under the influence of classical electrostatic field from the point charges of ~ 130 TIP3P waters within the potential cut-off sphere in the simulation box sampled in the course of the MC simulation. The coordinates of the three hydrogen atoms other than the transferring two protons in the solute **1–3** were not optimized in the computation of the potential surfaces (because geometry optimization under classical external point charges can be misleading). This may cause slight structural strain in the ionic states and thus small overestimate of the energy difference between the neutral and ionic states. However, we have expected error cancellation between this and small overestabilization of the ionic states in the simulation due to the RHF approximation employed for the charge determination. These two factors always tend to cancel each other rather than to accumulate. As mentioned in ref 42, very large calculations (of energy gradient and electron correlation) on a larger hydration cluster would be needed to quantify this issue.
- (46) We first fitted the simulation data of the free energy curves to two parabolas of an equal curvature, from which the solvent reorganization energy was calculated. The rms deviation of the fitting was about 0.9 kcal/mol.
- (47) This situation could be quite different in a small gas phase cluster situation as opposed to the present solution study. In the former, the bodily motion of e.g. a single solvating water molecule in switching its solvation from one of the reactant partners to another is quite important (see: Beksic, D.; Bertran, J.; Luch, J. M.; Hynes, J. T. *J. Phys. Chem. A* **1998**, *102*, 3977); in the present solution case, as in previous HCl studies (refs 10 and 11), small librational adjustments are involved with the nuclear center of masses of the solvating waters largely in place. It is also of interest to note that if the proton were to be treated (inappropriately) as a classical particle, then a variable more akin to a spatial gradient of ΔE would play a role (Hynes, J. T. In Simon, J. D., Ed.; *Ultrafast Dynamics of Chemical Systems*; Kluwer: Dordrecht, The Netherlands, 1994).
- (48) The continuous deformation of the proton potential curve as a function ΔE_{12} is described by an interpolation method outlined in the Appendix.

(49) The result of ΔG_{12}^{\ddagger} presented here is updated by improved (interpolation) calculations from the previous report in ref 12.

(50) Hammond, G. S. *J. Am. Chem. Soc.* **1955**, *77*, 334. Pross, A. *Adv. Phys. Org. Chem.* **1977**, *1*, 69.

(51) Kiefer, P.; Hynes, J. T. Manuscript in preparation.

(52) This denotes the mean-field parametrization of the electronic polarization of the TIP3P model for bulk water. We should also note that the nonpolarizable solvent models tend to overestimate the solvent reorganization energy. See e.g. ref 9.

(53) Agmon, N. *Chem. Phys. Lett.* **1995**, *244*, 456; *J. Chim. Phys. (Paris)* **1996**, *93*, 1714.

(54) Newton, M. D. *J. Chem. Phys.* **1977**, *67*, 5535.

(55) Reed, A. E.; Weinhold, F. *J. Chem. Phys.* **1983**, *78*, 4066. Reed, A. E.; Weinstock, R. B.; Weinhold, F. *J. Chem. Phys.* **1985**, *83*, 735.

(56) At and beyond $r_1 = 1.25$ Å, NBO analysis no longer assigns an F–H bond but instead a formation of an O–H bond in $F^{\cdots}H_3O^+$.

(57) The Monte Carlo sampled points of the free energy curves are again well approximated by parabolas with the rms deviation of 1.1 kcal/mol.

(58) A contrasting view would assume dominance of $H_5O_2^+$ structure around the excess proton rather than H_3O^+ . Although this issue is still under controversy, we point out here that theoretical or computational models having insufficient solvation (e.g., with small number of solvent molecules) would prefer the more charge delocalized form of $H_5O_2^+$. We also note that the second PT step is occurring in the presence of the F^- ion nearby, which can assist in localizing the proton compared to the case of proton transport in bulk water.

(59) Here we limit ourselves to a diabatic treatment, which is sufficient to clarify the issue.

(60) The activation energy ΔG^{\ddagger} is an increasing function of reorganization energy in a region where the reaction is endothermic and the endothermicity ΔG^0 is smaller than the reorganization energy.

(61) Antonchenko, V. Ya.; Davydov, A. S.; Zolotariuk, A. V. *Phys. Status. Solidi B* **1983**, *115*, 631. Davydov, A. S. *Solitons in molecular systems*; Naukovaja Dumka: Kiev, Ukraine, 1984. Godzik, A. *Chem. Phys. Lett.* **1990**, *171*, 217. For some recent reviews, see the articles by: Kryachko, E. S.; Sokhan, V. P. In ref 2b; Nagle, J. F. In ref 2b.

(62) The spectroscopic argument of ref 17 used to support the inherent stability of a contact ion pair for HF in water will be discussed elsewhere (ref 64a).

(63) Hammes-Schiffer, S.; Tully, J. C. *J. Chem. Phys.* **1995**, *103*, 8525; *J. Phys. Chem.* **1995**, *99*, 5793.

(64) (a) Schroeder, T.; Staib, A.; Hynes, J. T. Work in progress. (b) Ando, K.; Staib, A.; Hynes, J. T. In *Femtochemistry: Ultrafast Chemical and Physical Processes in Molecular Systems*; Chergui, M., Ed.; World Scientific: Singapore, 1996; p 534. Tramer, A., Ed. *Fast Elementary Processes in Chemical and Biological Systems*; AIP: New York, 1996; p 326.

(65) Luz, Z.; Meiboom, S. *J. Am. Chem. Soc.* **1964**, *86*, 4768.

(66) We have followed closely the screened Coulomb diffusion analysis of Eigen (ref 4) and do not repeat the equations; in brief, from kinetic measurements, Eigen et al. have evaluated the overall recombination rate for $F^- + H_3O^+$ to be $k_R = 1.0 \times 10^{11} \text{ M}^{-1} \text{ s}^{-1}$. By assuming the above-mentioned analysis applies (in the diffusion case) and using the dielectric constant of water $\epsilon = 79$, the diffusion constants of proton and F^- ions $D_{H^+} = 9.31 \times 10^{-5} \text{ cm}^2 \text{ s}^{-1}$ and $D_{F^-} = 1.46 \times 10^{-5} \text{ cm}^2 \text{ s}^{-1}$ (from the electrical mobility measurements), we obtain the recombination distance of 8.2 Å.

(67) Additional support, in the different context of halide ion–water complex IR spectra (Ayotte, P.; Bailey, C. G.; Weddle, G. H.; Johnson, M. A. *J. Phys. Chem. A* **1998**, *102*, 3067) can be found (Thompson, W. H.; Hynes, J. T. Unpublished work).